Vertical transport and processing of aerosols in a mixed-phase convective cloud and the feedback on cloud development

By Y. YIN[1,2]*, K. S. CARSLAW[1] and G. FEINGOLD[3]
[1]*Institute for Atmospheric Science, School of the Environment, University of Leeds, UK*
[2]*Institute of Mathematical and Physical Sciences, University of Wales Aberystwyth, UK*
[3]*NOAA, Environmental Technology Laboratory, USA*

SUMMARY

A modelling study of vertical transport and processing of sulphate aerosol by a mixed-phase convective cloud, and the feedback of the cloud-processed aerosols on the development of cloud microphysical properties and precipitation is presented. An axisymmetric dynamic cloud model with bin-resolved microphysics and aqueous-phase chemistry is developed and is used to examine the relative importance of microphysical and chemical processes on the aerosol budget, the fate of the aerosol material inside hydrometeors, and the size distributions of cloud-processed sulphate aerosols. Numerical simulations are conducted for a moderately deep convective cloud observed during the Cooperative Convective Precipitation Experiments. The results show that aerosol particles that have been transported from the boundary layer, detrained, and then re-entrained at midcloud levels account for a large fraction of the aerosol inside hydrometeors (∼40% by mass). Convective transport by the simulated cloud enhances upper-tropospheric aerosol number and mass concentrations by factors of 2–3 and 3–4, respectively. Sensitivity studies suggest that, for the simulated case, aqueous chemistry does not modify the evolution of the cloud significantly. Finally, ice-phase hydrometeor development is very sensitive to aerosol concentrations at midcloud levels. The latter result suggests that the occurrence of mid-tropospheric aerosol layers that have been advected through long-range transport could strongly affect cloud microphysical processes and precipitation formation.

KEYWORDS: Aerosol–cloud interaction   Bin microphysics model   Convective pumping   Deep convection

1. INTRODUCTION

The role of clouds in the scavenging, processing and transport of atmospheric aerosols has been appreciated and studied for a long time (e.g. Junge 1963; Hegg and Hobbs 1982; Rodhe 1983; Flossmann and Pruppacher 1988; Kleinman and Daum 1991; Bower and Choularton 1993; Feingold *et al.* 1996; Bower *et al.* 1997; Choularton *et al.* 1998; Wurzler *et al.* 2000; Feingold and Kreidenweis 2002). Most of these studies have concluded that in-cloud sulphate production adds mass effectively at sizes above the minimum activation radius achieved in the cloud, and that the enhancement will occur for particles on the order of 0.1 μm or larger. It has also been proposed that the collision–coalescence process has a similar effect on the increase in the cloud condensation nucleus (CCN) size as that due to sulphate production (Hudson 1993; Feingold *et al.* 1996). Most of the previous studies concerning cloud processing are restricted to liquid-phase clouds, especially to stratocumulus clouds, although it has been pointed out that the production of CCN by processing of aerosol in clouds with a vigorous updraught near cloud base (such as convective clouds) may be a more important source of CCN in the atmosphere (e.g. Choularton *et al.* 1998).

Mixed-phase convective clouds, especially deep convective clouds, have been recognized as an important means for vertical transport of pollutants from the planetary boundary layer to the upper troposphere (e.g. Dickerson *et al.* 1987; Prather and Jacob 1997; Yin *et al.* 2002a), but very little is known about how aerosols are processed, or how the aerosol size distribution and chemical composition are modified due to chemical and

* Corresponding author: Institute of Mathematical and Physical Sciences, University of Wales Aberystwyth, Aberystwyth, SY23 3BZ, UK. e-mail: yyy@aber.ac.uk

microphysical processes occurring in the course of transport. Previous studies indicate that cloud processing-induced modification of the CCN spectra could have important effects on subsequent cloud cycles (e.g. Wurzler *et al.* 2000), but the influence on the primary cloud cell of aerosol particles processed and detrained from itself has not been explored.

    In this study a dynamic cloud model with bin-resolving microphysics and aqueous phase chemistry of mixed-phase particles is developed and used to examine the relative importance of microphysical and chemical processes on aerosol scavenging, processing, and vertical redistribution. This study can be considered as an extension of the work of Respondek *et al.* (1995) who investigated the uptake, redistribution, and wet removal of $(NH_4)_2SO_4$ particles by a mixed-phase convective cloud. We will use the same thermodynamic profiles as used by Respondek *et al.* to initialize our model but will focus particularly on the effects of vertical transport, aqueous chemistry and microphysical processes on the aerosol size distribution and the feedback of modified aerosol on cloud development. In this paper, we restrict our analysis of cloud response to 'internal' aerosol changes (i.e. driven by the cloud's own dynamical and microphysical processes). The additional 'external' forcing by changes in the initial aerosol loading have received limited attention from others (e.g. Khain *et al.* 1999) and are also worthy of further investigations.

    In the following section the model is described, including a detailed description of the aqueous chemistry and aerosol treatment, which have been included since the studies of Yin *et al.* (2001, 2002a). Section 3 describes the initial conditions used in this study. In section 4, the main results are presented and discussed, while the main results are summarized in section 5.

2.   THE MODEL

    The model dynamics and microphysics are based on the axisymmetric non-hydrostatic cloud model of Reisin *et al.* (1996), which is an updated version of the one put forth by Tzivion *et al.* (1994), and are only briefly described here. Modifications to the microphysical processes, newly added scavenging processes and aqueous sulphur chemistry model will be given in more detail.

    A set of prognostic equations are solved for the vertical and radial velocity, the pressure perturbation, the virtual potential-temperature perturbation, the specific-humidity perturbation, the specific number concentration and mass of aerosol in a spectral bin, the specific number concentration and mass for each type of cloud particle in a size bin, and the concentration of activated ice nuclei.

    Four species of hydrometeor are considered: drops, ice crystals, graupel particles and aggregates (snowflakes). The density of the graupel is assumed to be 0.4 g cm^{-3}, while the ice crystal density varies from 0.9 g cm^{-3} for the smallest particles, down to 0.45 g cm^{-3} for the largest. The density of the aggregates is fixed at 0.2 g cm^{-3}. Each particle spectrum is divided into 34 bins with mass m doubling for adjacent bin boundaries ($m_{k+1} = 2m_k$, $k = 1, \ldots, 34$). The masses at the lower boundary of the first bin, m_1, and the larger boundary of the last bin, m_{35}, for both liquid and solid phases are 0.1598×10^{-13} and 0.17468×10^{-3} kg, which correspond to drop diameters of 3.125 and 8063 μm, and ice particle diameters of 3.23754 and 8540 μm, respectively. The density of aerosol is assumed equal to 2.0 g cm^{-3} and the aerosol spectrum is represented by 43 bins with radii ranging from 0.001 to 15.75 μm.

    The liquid-phase microphysical processes included are drop nucleation, condensation and evaporation, collision–coalescence, and binary break-up. The ice-phase

processes considered are ice nucleation (deposition, condensation–freezing, contact nucleation, and immersion freezing), ice multiplication, deposition and sublimation of ice particles, ice–ice and ice–drop interactions (coagulation, accretion, or riming), melting of ice particles, and sedimentation of drops and ice particles. All these microphysical processes are formulated for the first two moments (number and mass) of the distribution functions of each hydrometeor species and are solved using moment-conserving techniques (Tzivion *et al.* 1987; Feingold *et al.* 1988; Tzivion *et al.* 1989; Reisin *et al.* 1996).

In addition to prediction of the number concentration of aerosol particles, the present model also includes prognostic equations for the specific mass of aerosols in the air and in hydrometeors, and equations to describe impaction scavenging of aerosol particles by hydrometeors, aerosol regeneration following complete evaporation/sublimation of hydrometeors, gas–cloud interactions, and aqueous-phase oxidation of dissolved SO_2 by ozone and hydrogen peroxide. These will be described in more detail later.

The model domain is 12 km in the vertical and 6 km in the radial direction with an open lateral boundary at $r = R_{max}$, that is, $du/dr = dq/dr = 0$, where q represents any scalar, so that the scalars can transport freely across the boundary. The grid size is 300 m and 150 m, in the vertical and radial directions, respectively. A time step of 2.5 s is used for condensation/evaporation of drops or deposition/sublimation of ice particles, 0.01 s for gas absorption, and 5 s for all other processes.

(a) *Activation of aerosols*

The activation of aerosol particles to form cloud droplets (often referred to as nucleation scavenging) depends on the assumed aerosol composition and local supersaturation. In this study aerosol particles of a certain size are activated when the supersaturation calculated by the model at each grid point exceeds the critical value determined by the Köhler equation (Pruppacher and Klett 1997) assuming an $(NH_4)_2SO_4$ composition.

Aerosol particles begin to grow by absorption of water vapour long before they enter the cloud. These wetted particles provide the initial sizes for subsequent activation and condensational growth. In previous cloud models different schemes have been adopted to calculate the size of these wet particles. Mordy (1959) assumed that at cloud base 'wet' particles which formed on nuclei smaller than 0.12 μm were at equilibrium at 100% relative humidity (RH), and that particles formed on nuclei larger than 1.2 μm were at equilibrium at 99% RH. Flossmann *et al.* (1985) assumed that all the aerosol particles reached equilibrium with their environment at 99% RH. On the other hand, Kogan (1991) assumed that CCN with radii smaller than 0.12 μm formed initial droplets with sizes equal to the equilibrium radius at 100% RH, while for larger CCN the initial radii were specified as less than the equilibrium radii at 100% RH. Kogan introduced a factor k to indicate the size of the initial droplet relative to the size of the dry particle.

In this study a nucleation scheme similar to Kogan (1991) is used, except that a wider size range of aerosol is considered. Based on Mordy (1959) and Kogan (1991) we assume the condensation growth of aerosol particles with radii smaller than 0.12 μm to be according to the Köhler equation. After reaching the critical sizes, these particles are then transferred to the cloud droplet bins where their subsequent growth is calculated based on the kinetic condensation equation. For particles with radii larger than 0.12 μm, a factor k_{r_0} was used to calculate the initial sizes of the droplets at 100% RH ($k_{r_0} = 5.8w^{-0.12}a^{-0.214}$, with vertical velocity w in m s^{-1} and the particle radius a in μm; Kogan (1991)). The formulation of k indicates that the relative growth of a

particle decreases with both increasing particle size and increasing updraught, with w representing a proxy for time available for growth.

(b) Impaction scavenging of aerosols

Impaction scavenging of aerosol particles by hydrometeors leads to a decrease in the number concentration and mass of the aerosol particles in the air and to an increase in the corresponding values in the hydrometeors. This process also changes the distribution functions of the hydrometeors involved. For aerosol particles (in the air) with masses between $m_{ap,k}$ and $m_{ap,k+1}$ or radii between $r_{ap,k}$ and $r_{ap,k+1}$, the time rates of change of the number concentration N and specific mass M due to collection by hydrometeors can be expressed (e.g. Flossmann *et al.* 1985) as

$$\left(\frac{\partial N_{ap,k}}{\partial t}\right)_{ap,coll} = -\int_{m_{ap,k}}^{m_{ap,k+1}} f_{ap}(m_{ap})\,dm_{ap} \int_0^\infty f_h(m)\,K(m_{ap,m})\,dm, \qquad (1)$$

and

$$\left(\frac{\partial M_{ap,k}}{\partial t}\right)_{ap,coll} = -\int_{m_{ap,k}}^{m_{ap,k+1}} m_{ap} f_{ap}(m_{ap})\,dm_{ap} \int_0^\infty f_h(m)\,K(m_{ap},m)\,dm, \qquad (2)$$

respectively, where $f_{ap}(m_{ap})$ and $f_h(m)$ are the number density distribution functions of interstitial aerosol particles and cloud hydrometeors, respectively. $K(m_{ap},m)$ is the collection kernel:

$$K(m_{ap},m) = \pi(a + r_{ap})^2 E(m_{ap},m)|V_\infty(m) - V_\infty(m_{ap})|, \qquad (3)$$

where $E(m_{ap},m)$ is the collision efficiency with which an aerosol particle collides with a hydrometeor particle; $V_\infty(m)$ and $V_\infty(m_{ap})$ are the terminal velocities of hydrometeors and aerosol particles, respectively. As in other previous studies, the terminal velocities of aerosol particles are assumed negligible in the simulations.

The capture of aerosol particles also changes the size distributions of hydrometeor particles. The time rates of change of number concentration and specific mass of hydrometeors with mass between m_k and m_{k+1} can be written as

$$\begin{aligned}\left(\frac{\partial N_k}{\partial t}\right)_{ap,coll} &= \int_{m_k}^{m_{k+1}} \left(\frac{\partial f_h(m)}{\partial t}\right)_{ap,coll} dm \\ &= -\int_{m_k}^{m_{k+1}} \frac{\partial}{\partial m}\left\{\left(\frac{dm}{dt}\right)_{ap,coll} f_h(m)\right\} dm,\end{aligned} \qquad (4)$$

and

$$\begin{aligned}\left(\frac{\partial M_k}{\partial t}\right)_{ap,coll} &= \int_{m_k}^{m_{k+1}} m\left(\frac{\partial f_h(m)}{\partial t}\right)_{ap,coll} dm \\ &= -\int_{m_k}^{m_{k+1}} m\frac{\partial}{\partial m}\left\{\left(\frac{dm}{dt}\right)_{ap,coll} f_h(m)\right\} dm,\end{aligned} \qquad (5)$$

respectively, with

$$\left(\frac{dm}{dt}\right)_{ap,coll} = \int_0^\infty m_{ap} f_{ap}(m_{ap}) K(m_{ap,m})\,dm_{ap}. \qquad (6)$$

The time rate of change of the content of a specific chemical component i in a hydrometeor species h caused by collection of aerosol particles is expressed as

$$
\left(\frac{\partial S_{i,k}}{\partial t}\right)_{\text{ap,coll}} = \int_{m_k}^{m_{k+1}} \left(\frac{\partial s_{h,i}(m)}{\partial t}\right)_{\text{ap,coll}} \mathrm{d}m
$$

$$
= \int_{m_k}^{m_{k+1}} f_h(m)\,\mathrm{d}m \int_0^\infty s_{a,i}(m_{\text{ap}}) K(m_{\text{ap}}, m)\,\mathrm{d}m_{\text{ap}} \tag{7}
$$

$$
- \int_{m_k}^{m_{k+1}} \frac{\partial}{\partial m}\left\{\left(\frac{\mathrm{d}m}{\mathrm{d}t}\right)_{\text{ap,coll}} s_{h,i}(m)\right\}\,\mathrm{d}m,
$$

where $s_{a,i}$ and $s_{h,i}(m)$ are mass density distribution functions of chemical species i in unactivated aerosol and in hydrometeor species h, respectively. It should be noted that collection of aerosol by a hydrometeor species changes only the distribution of that hydrometeor: the total number concentration of the hydrometeor is not changed (total number is conserved). This can be proved by integrating Eq. (4) from 0 to ∞.

Equations (1)–(7) are solved numerically using the moment-conserving method of Tzivion *et al.* (1987). The values of the efficiencies for collision of drops with aerosol particles are based on Flossmann *et al.* (1985) and are derived from a combination of the theoretically computed values of Wang *et al.* (1978) and Beard and Grover (1974) for four different RH values (100%, 95%, 75% and 50%), with the experimental values of Wang and Pruppacher (1977). The efficiencies for the collision of ice crystals and snowflakes with aerosol particles are taken from the theoretical values of Martin *et al.* (1980) supplemented by the experimental values of Murakami *et al.* (1985). However, the efficiencies for collision of graupel particles with aerosol particles are assumed to be the same as those for collision of drops with aerosol particles, due to the lack of experimental and theoretical data (Alheit *et al.* 1990).

(c)   *Scavenging of trace gases*

To simulate the evolution of trace gases in the air and in hydrometeors, the dynamic and microphysical equations are also applied to the mixing ratio of a gas species i in the air, $M_{a,i}$, and the mixing ratio in hydrometeors, $M_{h,i}$. These equations are given as

$$
\frac{\partial M_{a,i}}{\partial t} = F_q(M_{a,i}) - D(M_{a,i}) + \left(\frac{\partial M_{a,i}}{\partial t}\right)_{\text{uptake}} + \left(\frac{\partial M_{a,i}}{\partial t}\right)_{\text{micro}} \tag{8}
$$

and

$$
\frac{\partial M_{h,i,k}}{\partial t} = F_q(M_{h,i,k}) - D(M_{h,i,k})
$$
$$
+ \left(\frac{\partial M_{h,i,k}}{\partial t}\right)_{\text{uptake}} + \left(\frac{\partial M_{h,i,k}}{\partial t}\right)_{\text{micro}} + \left(\frac{\partial M_{d,i,k}}{\partial t}\right)_{\text{chem}}, \tag{9}
$$

where the subscript k denotes the particle size bin number. The terms D and F_q represent the advective and turbulent transfer operators. The variation of these functions with location is implied. Also, the terms with subscripts 'uptake' and 'micro' represent mass transfer of chemical species between gas phase and condensed phase due to uptake of gases by drops and ice particles, and that between different particle types due to microphysical processes. All of these terms are calculated by solving the various kinetic equations (see Yin *et al.* 2001, 2002a). The term with subscripts 'chem' in Eq. (9)

TABLE 1.   EQUILIBRIUM REACTIONS AND REACTION CONSTANTS

Reaction	K_{298} (M or M atm^{-1})	$-\Delta H/R$ (K)	Reference
(R1) CO_2 (g) $\rightleftharpoons$ $CO_2 \cdot H_2O$	3.40×10^{-2}	2420	Smith and Martell (1976)
(R2) $CO_2 \cdot H_2O$ $\rightleftharpoons$ $HCO_3^- + H^+$	4.46×10^{-7}	-1000	Smith and Martell (1976)
(R3) $HCO_3^- \rightleftharpoons CO_3^{2-} + H^+$	4.68×10^{-11}	-1760	Smith and Martell (1976)
(R4) SO_2 (g) $\rightleftharpoons SO_2 \cdot H_2O$	1.4	3120	Lide and Frederikse (1995)
(R5) $SO_2 \cdot H_2O \rightleftharpoons HSO_3^- + H^+$	1.23×10^{-2}	1960	Smith and Martell (1976)
(R6) $HSO_3^- \rightleftharpoons SO_3^{2-} + H^+$	6.61×10^{-8}	1500	Smith and Martell (1976)
(R7) H_2O_2 (g) $\rightleftharpoons H_2O_2$ (aq)	8.3×10^4	7400	O'Sullivan *et al.* (1996)
(R8) O_3 (g) $\rightleftharpoons O_3$ (aq)	1.1×10^{-2}	2400	Jacob (1986)
(R9) H_2SO_4(aq) $\rightleftharpoons HSO_4^- + H^+$	1000		Perrin (1982)
(R10) $HSO_4^- \rightleftharpoons SO_4^{2-} + H^+$	1.02×10^{-2}	2720	Smith and Martell (1976)
(R11) $H_2O \rightleftharpoons H^+ + OH^-$	1.0×10^{-14}	-6710	Smith and Martell (1976)

The temperature dependence is represented by van't Hoff's relation: $K_T = K_{298} \exp\{(-\Delta H/R)(1/T - 1/298)\}$, where H is enthalpy, R is the universal gas constant and T is temperature (K).

represents chemical transfer between different species due to aqueous phase reactions such as oxidation of S(IV) to S(VI) in drops, which will be described in detail in the following section. As drops evaporate, the aqueous phase concentrations of the dissolved gases are recalculated for the new water content and this concentration is used to determine the new evaporation/condensation rate of the gas. For sublimation of ice particles, the buried gas species is released to the gas phase at a rate proportional to the mass of water evaporated (Yin *et al.* 2002a).

During drop freezing or riming, a fraction of the gases originally dissolved in the drops will revert back to the gas phase. The retention coefficient, which is the ratio of the concentration of solute retained in the ice phase to that in the parent liquid phase, has a significant influence on the gas redistribution and has been investigated by many researchers (see Yin *et al.* (2002a) for a review). In the present study 30% of H_2O_2, a value measured by Snider *et al.* (1992) in natural clouds, and 38% of SO_2 (based on the measurement of Iribarne *et al.* 1990) dissolved in the drops will be released back to the air during conversion of drops to ice particles via the various freezing processes. Other gaseous species involved in this study, O_3 and CO_2, are assumed completely released when drops freeze due to lack of measurement data and their relatively low solubility. It should be noted that the dissolution of gases into drops is calculated kinetically, so that, depending on the species, the gas concentrations dissolved may or may not be the equilibrium values during freezing.

(d)   Aqueous sulphate chemistry and droplet acidity

Four gas species are considered in this study, and the equilibrium reactions in water and the reaction constants are listed in Table 1, where the temperature dependence is represented by van't Hoff's relation:

$$K_T = K_{298} \exp\left\{ \frac{-\Delta H}{R} \left(\frac{1}{T} - \frac{1}{298} \right) \right\},$$

where ΔH is the enthalpy change for the equilibrium relations involved, R is the universal gas constant and T is temperature (K).

The model includes the following oxidation mechanisms of S(IV) to S(VI):

$$S(IV) + H_2O_2 \rightarrow S(VI) + H_2O, \tag{R12}$$

TABLE 2.   CONSTANTS FOR AQUEOUS-PHASE OXIDATION REACTIONS

Constant	K_{298} (M^{-1}s^{-1})	$-E/R$ (K)	Reference
k_0	$2.4 \times 10^{+4}$	–	Hoffmann and Calvert (1985)
k_1	$3.7 \times 10^{+5}$	-5530	Hoffmann and Calvert (1985)
k_2	$1.5 \times 10^{+9}$	-5280	Hoffmann and Calvert (1985)
k_4	$7.5 \times 10^{+7}$	-4430	McArdle and Hoffmann (1983)

The temperature dependence is represented by $K_T = K_{298} \exp\{(-E/R)(1/T - 1/298)\}$, where E is collision efficiency, R is the universal gas constant and T is temperature (K).

$$S(IV) + O_3 \rightarrow S(VI) + O_2. \tag{R13}$$

The reaction rates of (R12) and (R13) are pH-dependent and are calculated as follows (Seinfeld and Pandis 1998): oxidation by O_3

$$-\frac{d[S(IV)]}{dt} = (k_0[SO_2 \cdot H_2O] + k_1[HSO_3^-] + k_2[SO_3^{2-}])[O_3]; \tag{10}$$

oxidation by H_2O_2

$$-\frac{d[S(IV)]}{dt} = \frac{k_4[H^+][H_2O_2][HSO_3^-]}{1 + 13[H^+]}, \tag{11}$$

where, k_0, k_1, k_2, and k_4 are the reaction constants (Table 2). We recognize the importance of metal ions catalysed oxidation of S(IV) on sulphate production, especially under weak acidity conditions (e.g. Kreidenweis *et al.* 1997). However, due to the lack of knowledge of the distribution of metal ions in the spectrum of aerosol particles, these oxidation reactions are not included in the present study. In addition, dilute solution chemistry is assumed for all the aqueous chemical reactions in drops, and the reactions are terminated if the liquid-water content in a drop bin is less than 10^{-10} kg kg^{-1}, which is equivalent to one droplet per litre of air in the first bin. The water produced in chemical reaction (R12) has been neglected from the water budget because it is so small compared to the cloud liquid-water content.

The hydrogen ion concentration in the droplets affects the uptake rate of SO_2 as well as the reaction rates above. The acidity or hydrogen ion concentration, $[H^+]$, is calculated for each size bin of drops based on an electroneutrality relationship:

$$\begin{aligned}
[H^+] = [C(IV)] &\frac{K_{R2}([H^+] + 2K_{R3})}{[H^+]^2 + [H^+]K_{R2} + K_{R2}K_{R3}} \\
+ [S(IV)] &\frac{K_{R5}([H^+] + 2K_{R6})}{[H^+]^2 + [H^+]K_{R5} + K_{R5}K_{R6}} \\
+ [S(VI)] &\frac{K_{R9}([H^+] + 2K_{R10})}{[H^+]^2 + [H^+]K_{R9} + K_{R9}K_{R10}} + \frac{K_{R11}}{[H^+]}.
\end{aligned} \tag{12}$$

Here K_i are equilibrium constants and subscripts denote reaction as given in Table 1. This equation is solved numerically at each time step.

(e)   Regeneration of aerosol particles

Aerosol particles are regenerated following complete evaporation of cloud particles. This process is important since both the sizes and chemical compositions of the regenerated particles could be considerably different from those unaffected by the cloud, and

thus influence the microphysical and optical properties of the clouds developed subsequently. For warm clouds one can assume that one cloud drop produces one aerosol particle based on experimental studies (e.g. Mitra *et al.* 1992). We also assume that one ice hydrometeor particle produces one aerosol particle. We have tested the validity of this assumption by regenerating as many as 10 particles per evaporated ice crystal, but this does not greatly affect aerosol concentrations in these particular simulations because the concentration of ice crystals is two to three orders less than the ambient aerosol concentrations.

During cloud development, hydrometeors in a single size bin scavenge aerosol particles of different sizes and absorb SO_2, which leads to an increase in aerosol mass in that bin. Collision and coalescence between different hydrometeors also changes the aerosol mass in a given hydrometeor bin. It is impractical in such a model to track the size distribution of the aerosol within a given single size bin of the hydrometeor distribution. Therefore we calculate only the total aerosol mass in each hydrometeor bin. Additional information on the aerosol concentration can be derived indirectly from the fact that, in the multi-moment approach, drop number is also prognosed (see Feingold *et al.* 1996). Upon complete hydrometeor evaporation we assume that the aerosol particles regenerated by a hydrometeor species at each time step are distributed as a log-normal function with the geometric standard deviation equal to the mean value of the three log-normal distribution functions of initial aerosol conditions (see section 3). Separate tests have also been conducted by assuming gamma distribution functions or a single size with the diameter equal to the volume-mean diameter of all the regenerated particles (see section 4(d)).

Our model necessarily makes assumptions about the size distribution of the detrained aerosol. Other studies in which the aerosol distribution is tracked in single air parcels using Lagrangian models capture the changes in distribution accurately but, because their dynamics are prescribed, do not capture the re-entrainment and feedback on cloud development. The inability to maintain full aerosol size information during evaporation is an inherent problem of Eulerian microphysical models that do not carry a full aerosol size distribution in each hydrometeor size bin. Nevertheless, we note that the microphysical treatment of the aerosol employed here has been designed to ensure a domain-wide conservation of aerosol mass and number. Furthermore, high fidelity in local features of the size distribution is ensured (as will be shown in Fig. 7) because of (i) the inclusion of prognostic equations for aerosol mass and number, as well as the mass of soluble material in hydrometeors; and (ii) the mass and number-conserving regeneration scheme. The same approach was used successfully in Feingold and Kreidenweis (2002) where it was shown that the general features of shifts in aerosol size due to processing are quite well represented by this method.

3.   INITIAL CONDITIONS AND DESCRIPTION OF DIFFERENT SIMULATIONS

(a)   Meteorology

The temperature and humidity profiles obtained during the Cooperative Convective Precipitation Experiment (CCOPE) on 19 July 1981 in Miles City, Montana, are used to initiate our model. The atmospheric conditions on that day were characterized by moderate instability and relatively weak shear and were favourable for development of local convection with limited precipitation. The relatively weak wind shear was also a particularly favourable condition for numerical simulations using an axisymmetric cloud model, in which the influence of environmental wind shear cannot be included. The profiles of temperature and dew-point temperature, shown in Fig. 1(a), represent
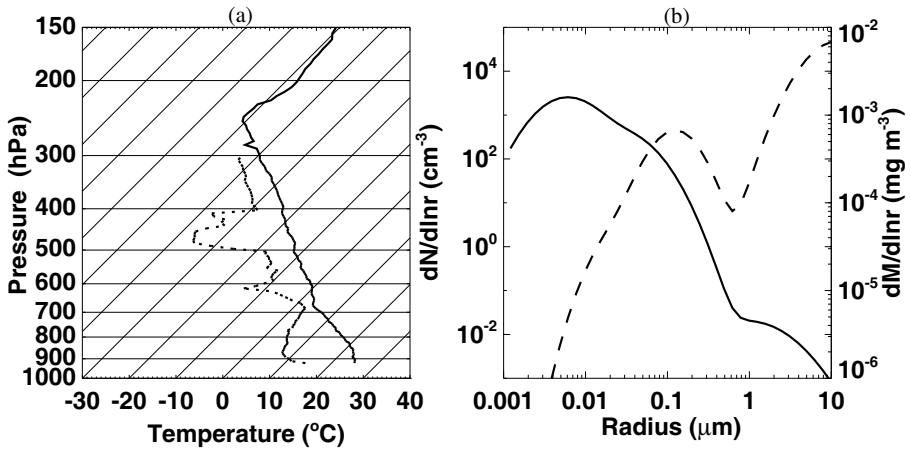
Figure 1.   (a) The 1440 MDT (2040 UTC) Miles City, Montana, USA, sounding of temperature (solid curve) and dew-point temperature (dashed curve) for 19 July 1981, and (b) initial number (solid curve) and mass (dashed curve) density distribution functions of aerosol particles (based on Hobbs *et al.* (1985) and Respondek *et al.* (1995)) used in the simulations (only the soluble particles are shown).

the atmosphere approximately 1.5 hours prior to the formation of the observed cloud and were taken approximately 35 km to the east of the observation area (the original sounding was modified to make the lowest layers adiabatic). For initialization, a warm bubble that produced a 2 degC perturbation was applied for one time step at $t = 0$ in a region with radial distance of 450 m, at the lower left corner of the domain.

The meteorological and cloud microphysical conditions on 19 July were well measured and reported by Dye *et al.* (1986), and have been simulated by many authors (e.g. Helsdon and Farley 1987; Murakami 1990; Respondek *et al.* 1995; Taylor *et al.* 1997) using models of different sophistication.

(b)   *Aerosols and trace gases*

The size distribution, concentration and chemical composition of aerosol particles were available at the site (Hobbs *et al.* 1985) but unfortunately not for the same date. The aerosol distribution of Hobbs *et al.* (1985) was fitted by superimposing three log-normal distribution functions as

$$\frac{\mathrm{d}N}{\mathrm{d}\ln r_n} = \sum_{i=1}^{3} \frac{n_i}{(2\pi)^{1/2} \log \sigma_i \ln 10} \exp \left[-\frac{\{\log(r_n/R_i)\}^2}{2(\log \sigma_i)^2} \right], \qquad (13)$$

where r_n is the radius of aerosol particles, n_i the total number of aerosol particles, R_i the geometric mean aerosol particle radius, and σ_i the standard deviation in mode i, using the parameters provided by Respondek *et al.* (1995). Based on the measurements of Hobbs *et al.* (1985), we assumed an external mixture such that 15% of the aerosol particles by number were water soluble, and that the soluble aerosols were composed of ammonium sulphate, regardless of size. The aerosol concentration is assumed to decrease exponentially with altitude with a scale height of 2 km (e.g. Pruppacher and Klett 1997). The vertical profile of aerosol concentration varies widely between different global regions and no single profile can be considered as generally applicable. In later parts of this paper we highlight the results that will be sensitive to the particular aerosol profile. The total number and mass concentrations of sulphate particles at the surface

TABLE 3. INITIAL FIELDS OF TRACE SPECIES CONSIDERED IN THIS STUDY

Species	Clean air (Surface value)	Polluted air (Surface value)	Scale-height
CO_2	330 ppmv	330 ppmv	Constant with altitude
SO_2	2 ppbv	10 ppbv	2.0 km
O_3	50 ppbv	50 ppbv	Constant with altitude
H_2O_2	0.5 ppbv	1 ppbv	Constant with altitude

TABLE 4. NUMERICAL EXPERIMENTS CONDUCTED IN THIS STUDY

Case	Initial gas condition	Aqueous chemistry	Aerosol regeneration
Base	Clean	Yes	Yes
ST1	Clean	No	Yes
ST2	Polluted	Yes	Yes
ST3	Clean	Yes	No

The initial trace gas fields under clean and polluted conditions are given in Table 3.

are 4280 cm^{-3} and 11 $\mu g\ kg^{-1}$, respectively. The initial number and mass distributions of the soluble aerosol particles used in this study are shown in Fig. 1(b).

There are no measurements of chemical species during the CCOPE field experiment. In order to investigate how our model results are sensitive to the initial chemical concentration, two scenarios are assumed to represent a clean and a polluted air mass, respectively. Table 3 lists the initial surface values of different trace species and the applied scale-height in the two cases. The values of SO_2, H_2O_2, and O_3 concentrations for the base case are similar to those used by Kreidenweis *et al.* (1997) and are in agreement with observations (e.g. Georgii and Meixner 1980; Luke *et al.* 1992) and other model studies (e.g. Yuen *et al.* 1994).

(c) *Description of different model runs*

Four different model simulations have been run to examine the sensitivity of cloud development to the SO_2 concentrations and the degree to which the cloud-processed aerosol can affect the primary cloud (Table 4).

The base case (described previously) represents an unpolluted situation in which the cloud-processed aerosols are allowed to feedback on the cloud microphysics. In the sensitivity test (ST1), we explore the role played by changes in chemistry (SO_2 uptake and oxidation) in driving changes in cloud-processed aerosol. We do this by repeating the base case but excluding aqueous chemical reactions as a production mechanism for aerosol sulphate mass. Case ST2 has a higher SO_2 concentration, while in ST3 regeneration of aerosol particles following complete evaporation of hydrometeor particles has been switched off, thereby removing the feedback of processed aerosol on cloud development.

4. RESULTS AND DISCUSSIONS

(a) *General characteristics of the model cloud and comparison with observations*

Figure 2 shows the time evolution of the maximum values of water content and number concentration of drops and ice-phase particles, vertical velocity and reflectivity
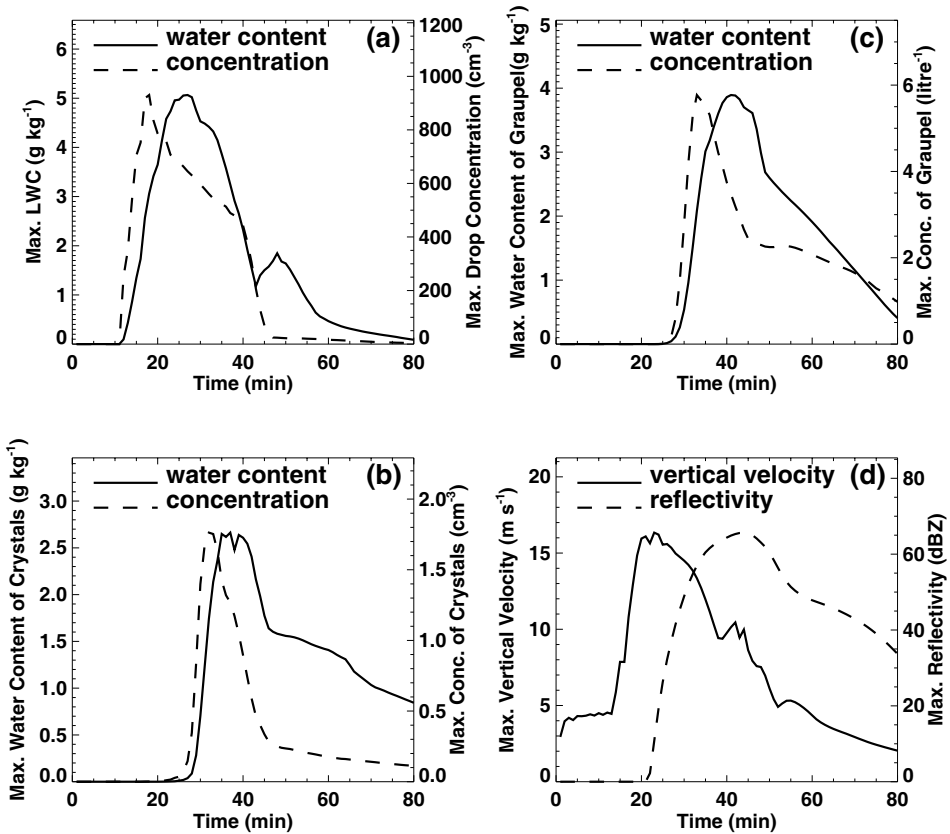
Figure 2.   Time-evolution of the maximum values of (a) liquid-water content and number concentration of drops, (b) ice-water content and number concentration of crystals, (c) ice-water content and number concentration of graupel particles, and (d) vertical velocity and reflectivity in the simulation.

in the base case and, as an example, the spatial distributions of hydrometeors and wind field at different stages of cloud development are shown in Fig. 3. We can see that the vertical velocity remained small (less than 5 m s^{-1}) until 15 min. Thereafter, especially from 17 to 27 min of the simulation, the cloud experienced an explosive developing phase, and reached the peak updraught speed of 16.3 m s^{-1} at a height of 6 km, after 24 min of simulation. (All altitudes in this paper are given in km above mean sea level, MSL, and the height of the topography is 0.8 km MSL.)

In order to directly compare our model results with the observations of Dye *et al.* (1986) we have established a timing reference between the model and the natural cloud: that is, $t = 0$ for the simulation refers to 1600 MDT (MDT = UTC −6 h) in the natural cloud. This choice is based mainly on the time of the vigorous development of updraught and cloud drops, and therefore the shallow and less-vigorous cloud that existed prior to 1600 MDT was not simulated here.

Table 5 summarizes a quantitative comparison of the cloud appearance and microphysical properties between the model cloud and the observations reported by Dye *et al.* (1986). From this table we can see that our model reproduced reasonably well the cloud-base height, size of the main updraught core, updraught speed at cloud base, the start time of the updraught decay, the location and time of the maximum liquid-water content, the concentration of droplets, the first appearance of graupel, and the first radar echo.
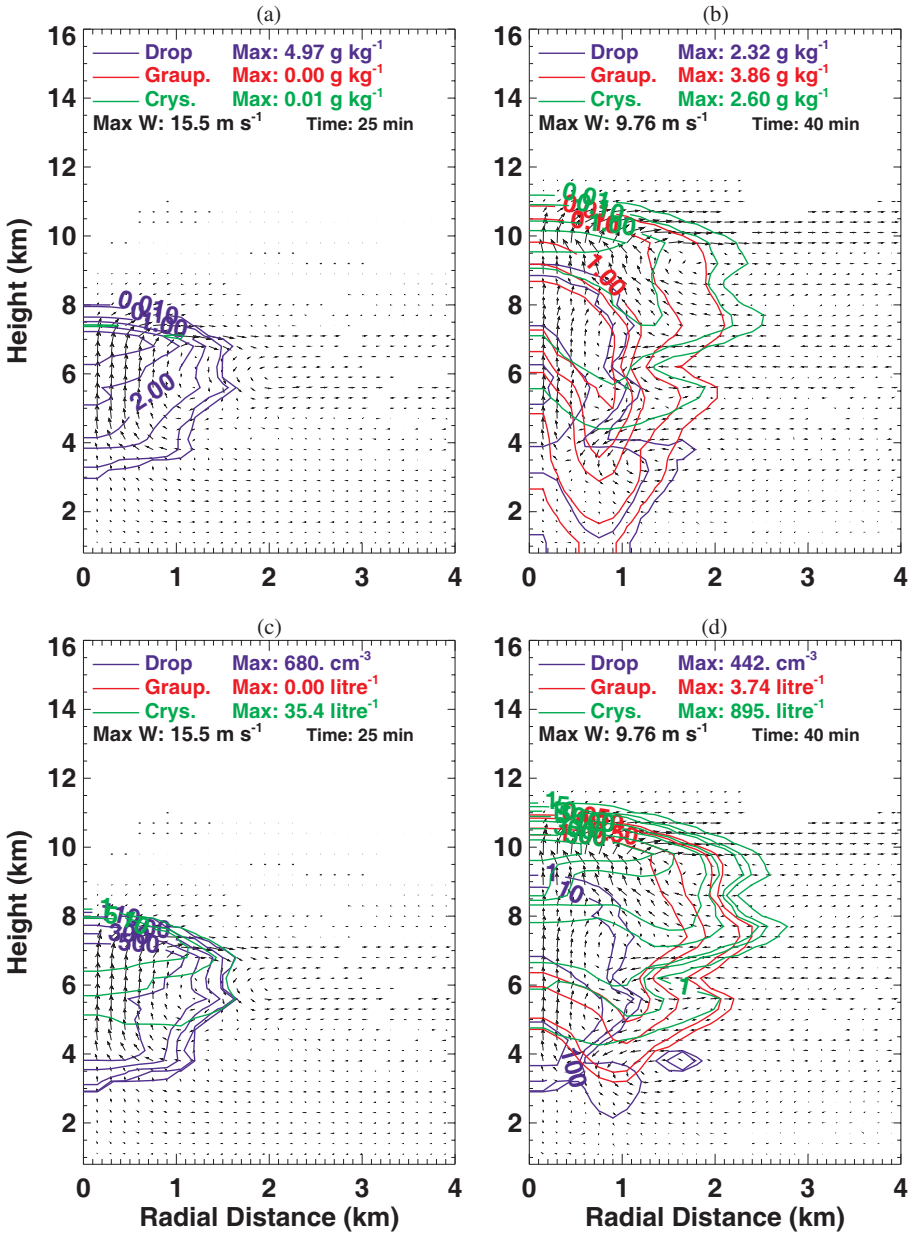
Figure 3. Spatial distributions of (a) and (b) specific mass, and (c) and (d) number concentration for drops, graupel and ice crystals at 'cumulus stage' (at 25 minutes) characterized by an updraught, velocity w, throughout most of the cell, and 'mature stage' (at 40 minutes) characterized by the presence of downdraughts and updraughts. Arrows are wind vectors.

TABLE 5. QUANTITATIVE COMPARISONS OF MODEL RESULTS WITH THE OBSERVATIONS OF DYE *et al.* (1986)

	Model		Observation	
Feature	Value	Time	Value	Time
GENERAL CLOUD APPEARANCE				
Cloud-base height	3.5–3.8 km	–	3.9 km	–
Maximum cloud-top height	11.5 km	–	10.5 km	–
Updraught width	2 km	–	2 km	–
Cloud diameter	5 km	–	6 km	–
Maximum vertical velocity	16.3 m s^{-1}	–	15 m s^{-1}	–
	at 6 km	1624	at 6.5 km	1627
Cloud-base updraught	$1–6 \text{ m s}^{-1}$	–	$1–5 \text{ m s}^{-1}$	–
Updraught decay starts	–	1632	–	1632–1634
DEVELOPMENT OF HYDROMETEORS				
Liquid-water content (g m^{-3})	0.9–2.6	1620–1626	1.0–2.2	1620–1626
around 6 km	<0.01	1647–1651	0.04–0.06	1647–1651
Drop concentration (cm^{-3})	930 (4.1 km)	1618	800–900	1619
	603 (5.9 km)	1625	600	1625
Concentration of ice	0.57–6.00	1620–1623	0.6	1620–1623
particles (l^{-1}) at 6 km	7	1626	5	1626
	15	1648	64	1648
	11	1651	45	1651
First graupel, at 5.8 km	0.01 l^{-1}	1626	single (3.6 mm)	1626
First radar echo (5 dBZ)	6–7 km	1623	7 km	1623

All altitudes are given in km above mean sea level, and times in Mountain Daylight Time (MDT = UTC −6 h).

The modelled maximum cloud-top height, 11.5 km, was about 1 km higher than the observation, and the mean cloud diameter was 1 km narrower for the model cloud. The concentrations of ice crystals in the model cloud are lower than the *in situ* measurements at the levels where the 'King Air' aircraft made penetrations of the cloud, but from Fig. 3 it is seen that the concentration of ice crystals in the simulated cloud is much higher at higher altitudes. Nevertheless, the model's ability to reproduce the main characteristics of the natural cloud gives us the confidence to use it as a framework for investigating the microphysical and chemical aspects of cloud processing and redistribution of aerosol particles and trace species.

(b)   *Scavenging, redistribution and processing of sulphate particles*

To understand the relative importance of various physical and chemical processes on aerosol populations, Fig. 4 shows the rates of change of aerosol mass due to various processes in the cloud. The rates are shown as height–time slices integrated across each cloud level. Table 6 lists the absolute and relative (in percentages) integrated contributions of these processes at the end of the runs (80 min). Nucleation and impaction scavenging, and S(IV) oxidation, are processes that increase aerosol mass inside hydrometeors, while precipitation and complete evaporation are processes that reduce the aerosol mass in hydrometeors. From Fig. 4 it is clear that nucleation scavenging (drop activation) dominates in-cloud scavenging, and is the fastest process for uptake of aerosol mass from the atmosphere, especially in the lower part of the cloud during the rapid development stage (17–27 min). On the other hand, impaction scavenging by drops (which also includes melted ice-phase hydrometeors) or graupel particles, is more important for below-cloud-base scavenging. In-cloud impaction scavenging of the smallest aerosol particles is also very efficient. These results are consistent with previous
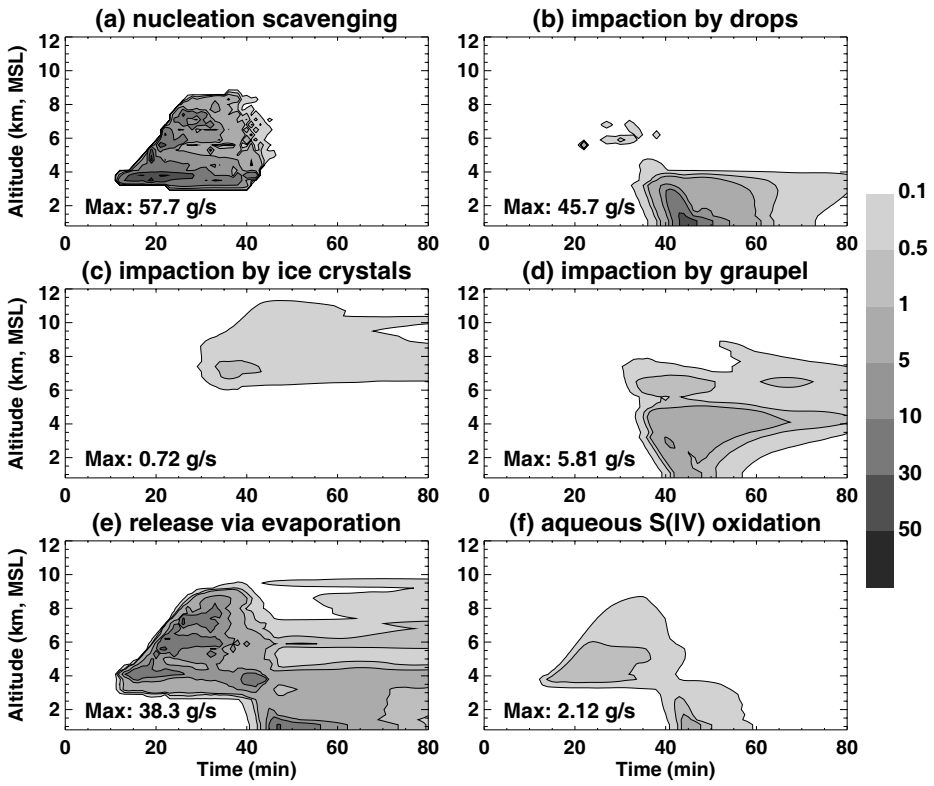
Figure 4.   Rates of: (a) nucleation scavenging; impaction scavenging of (b) drops, (c) ice crystals and (d) graupel particles; (e) regeneration via complete evaporation of hydrometeors; (f) sulphate production in aqueous phase via oxidation of SO_2. The results are shown for the base case, and are presented as a function of time and altitude (MSL) with masses summed across each model layer.

TABLE 6.   CONTRIBUTIONS OF VARIOUS PROCESSES TO AEROSOL MASS IN HYDROMETEORS

Definition	Base Case	ST1	ST2	ST3
Nucleation	256.4 (60.2)	251.7 (61.8)	287.6 (53.8)	152.2 (42.3)
Impaction by drops	95.5 (22.4)	95.4 (23.4)	95.8 (17.9)	117.4 (32.6)
Impaction by crystals	11.3 (2.6)	11.2 (2.8)	11.4 (2.1)	9.6 (2.7)
Impaction by graupel	49.2 (11.5)	49.1 (12.1)	49.8 (9.3)	65.2 (18.1)
S(IV) oxidation	13.6 (3.2)	0.0 (0.0)	89.9 (16.8)	15.3 (4.3)
Evaporation	281.7 (66.1)	268.4 (65.9)	363.3 (68.0)	0.0 (0.0)
Wet deposition	113.4 (26.6)	109.1 (26.8)	137.2 (25.7)	128.1 (35.6)
Aerosol mass remaining in hydrometeors	12.9 (3.0)	12.9 (3.2)	12.9 (2.4)	13.7 (3.8)

The unit is kg. The values in brackets are the relative contributions (percentages) of an individual process to the total aerosol mass gain in hydrometeors. The values are shown for the base case, and sensitivity cases ST1, ST2 and ST3 (see text for more explanation about case definition), after 80 min of simulations. 'Total aerosol mass gain' is defined as the total aerosol mass inside hydrometeors obtained by nucleation, impaction and SO_2 oxidation.

modelling studies (e.g. Jensen and Charlson 1984; Flossmann and Pruppacher 1988) and field observations (e.g. Hegg *et al.* 1984; Schumann *et al.* 1988).

It is also apparent from Fig. 4(a) that nucleation scavenging takes place not only in the region near the cloud base but also in regions up to a few kilometres above. Such in-cloud activation has been suggested as a possible mechanism for broadening
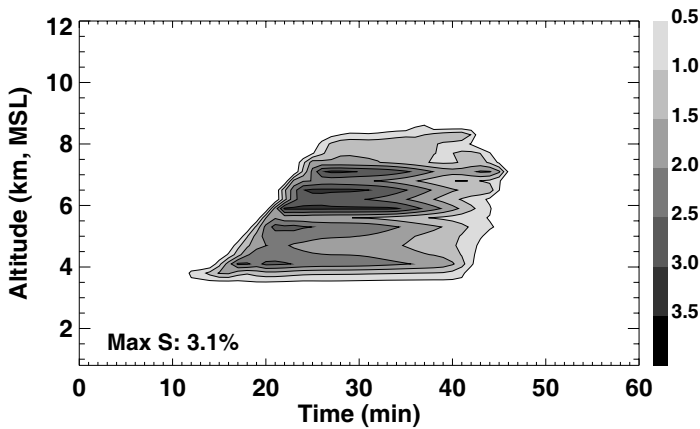
Figure 5.   Time evolution of maximum supersaturation (%) as a function of altitude.

the cloud-drop spectrum (Pinsky and Khain 2002). To further explore the reason for the in-cloud activation in this simulation, Fig. 5 shows the maximum supersaturation, which is obtained at each time step before drop activation, as a function of time and altitude. It is clear that, after the main activation pulse at low levels, the supersaturation increases with height due to the increase in vertical velocity and decrease in aerosol concentration. The supersaturation at 6 km height eventually exceeds that at cloud base after 23 min simulation. Re-entrainment of cloud-processed aerosol particles also enhances in-cloud activation because the processing transforms small aerosol to sizes where they could be more efficient CCN. However, the mechanism suggested by Pinsky and Khain is difficult to verify since the formation of precipitation particles in this particular cloud is dominated by cold cloud processes (Dye *et al.* 1986).

    Figure 6 shows the vertical distributions of normalized (with respect to the initial surface value) aerosol mass and number in the core updraught area at different modelling times in the base case. (The core updraught area is defined as the central cloud column with radial distance of 1 km.) It is seen that aerosol particles in the cloud region from 3.8 to 7.5 km are almost depleted by nucleation scavenging (refer to the curves for mass), during the cloud developing stage (30 min in the figure). Only the smallest particles, which account for a small fraction of the total mass, are left as interstitial particles (Fig. 6(b)). These are further reduced by in-cloud impaction scavenging. This can also be seen from the aerosol distributions shown in Fig. 7. At later times (40–70 min) aerosol loading in this layer is partially recovered due to convective transport of aerosol from the surface and lateral mixing. This is accompanied by significant removal of aerosol particles from the lower cloud region (below 6 km) and below the cloud by precipitation. Also noticeable is an increase in the aerosol loading at the cloud-top layer due to vertical transport. After precipitation (70 min in Fig. 6), aerosol loading in the layer from cloud base (around 3.8 km) to 7 km is reduced by 20–50%, and in the below-cloud layer by 30–70%. But this is more than doubled near the cloud top (around 11 km). This disturbance of the upper-tropospheric sulphate aerosol loading could play an important role in radiative forcing and heterogeneous chemistry, although the impact at any one location will depend on the vertical profile of aerosol mass and number.
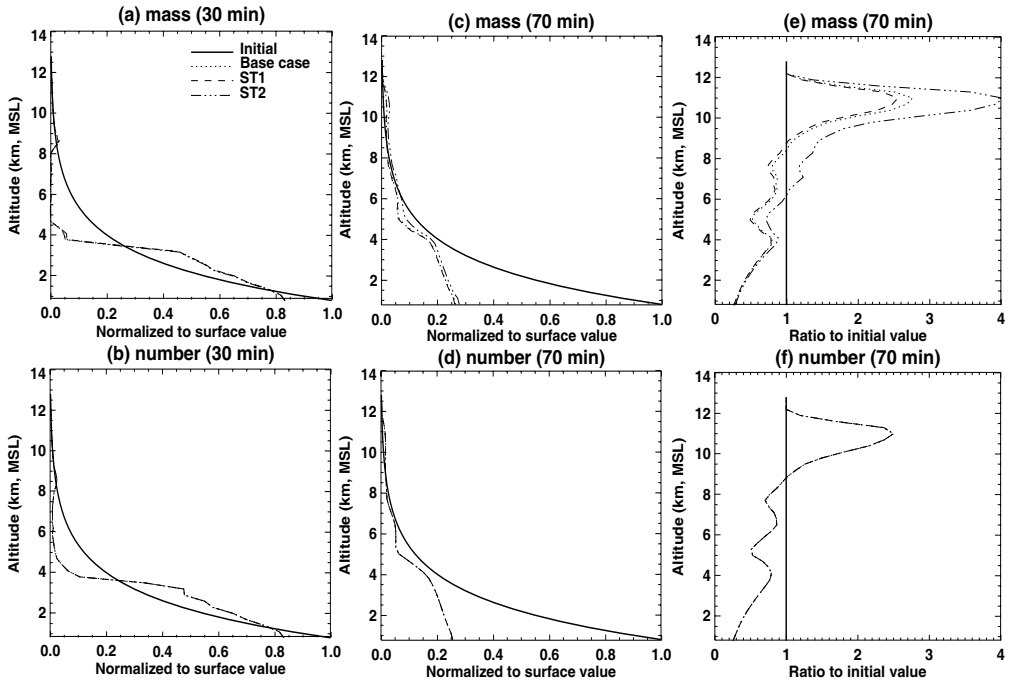
Figure 6.   Vertical distributions of: (a), (c) and (e) aerosol mass, and (b), (d) and (f) number, in the core updraught area of the base case and sensitivity cases ST1 and ST2 after 30 and 70 min simulation, respectively. (a)–(d) show the normalized distributions with respect to initial surface values, while (e) and (f) give the distributions as a ratio of the initial values. The core updraught area is defined as a column with radial distance of 1 km in the cloud centre. As a comparison, the initial background distribution is also given. Note that in some cases differences between the base case, ST1 and ST2 are too small to differentiate.

(c)   *Effects of aqueous sulphate production*

Sulphur dioxide is oxidized in the droplets leading to the production of SO_4^{2-}, which adds to the aerosol mass. Cloud-processed aerosols are produced by complete evaporation of sulphate-containing hydrometeors at the cloud edges and cloud top. As an example, Fig. 7 shows the size distribution functions of aerosol mass and number at different locations after 30 min simulation, compared with the initial distributions. This figure indicates that, in the core updraught region, sulphate particles with diameters larger than about 0.02 μm are depleted via nucleation scavenging; however, the distributions in the cloud lateral boundary region and the cloud-top layer indicate an increase in both the mass and number concentration of aerosol particles larger than 0.03 μm in diameter, especially for particles larger than 0.1 μm. When these cloud-processed aerosols re-enter the cloud updraught region at a later time, either by convergence or entrainment or both, their increased size allows them to be more effective CCN than unprocessed particles. As noted in section 2(e), the shift to larger sizes is only simulated in an approximate fashion but we will show later that this does not affect our results.

To examine the extent to which aqueous chemistry processing may affect the cloud evolution we performed a sensitivity test, ST1, in which aqueous chemistry was not simulated. Close examination of the results shows only minor differences from the base case, indicating that the sulphate mass added to the processed aerosols does not have a substantial effect on the cloud when these aerosols re-enter the cloud. A further sensitivity test, ST2, in which the SO_2 concentration is increased to 10 ppbv (versus
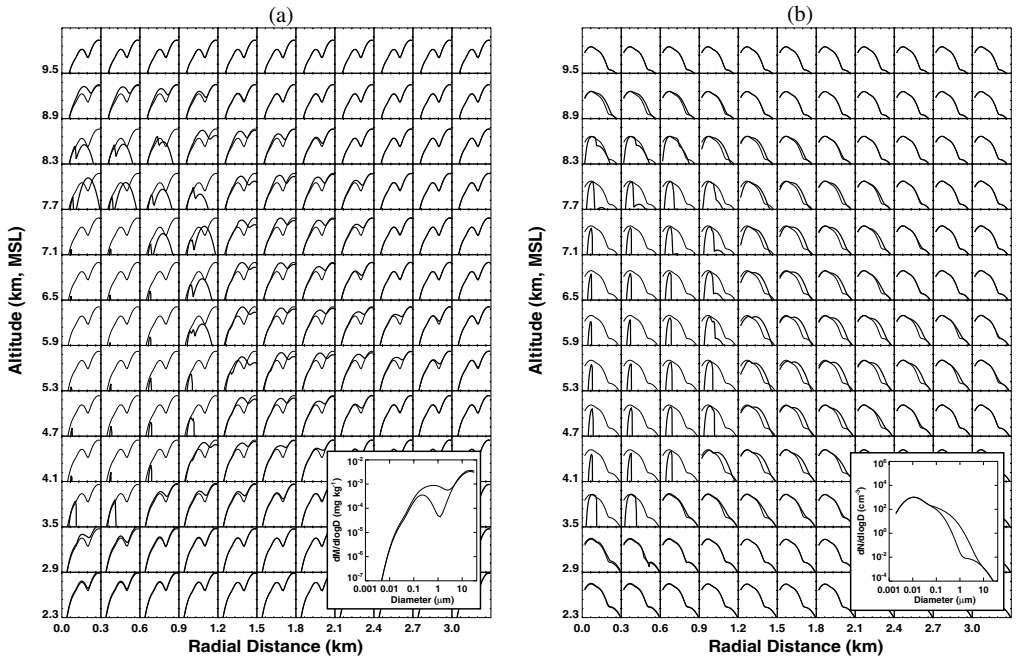
Figure 7.   Spatial and spectral distributions of (a) specific mass (mg kg^{-1}) and (b) number concentration (cm^{-3}), of aerosol particles after 30 min of simulation. The initial background values are shown as thin curves. Overlapping curves indicate that the aerosol distribution has not changed. For clarity, one of the distributions is enlarged and is shown at the lower right corner.

2 ppbv in the base case) and H$_2$O$_2$ is doubled to 1 ppbv, also shows small changes from the base case and confirms that aqueous chemistry does not significantly affect cloud evolution during the course of the simulation. Table 6 compares the contributions of various processes to aerosol mass in the hydrometeors and shows that, even in the high SO$_2$ case ST2, in-cloud oxidation accounts for only ∼17% of the total aerosol mass transfer into hydrometeors, indicating that gas scavenging is of secondary importance to the overall aerosol mass in hydrometeors. The relative unimportance of gas scavenging in the processing of aerosol particles has also been found by Hatzianastassiou *et al.* (1998) for a warm marine cumulus cloud. On the other hand, Feingold and Kreidenweis (2002) showed that sulphate production may alter the dynamics and precipitation in a shallow marine stratocumulus cloud.

(d)   Re-entrainment and activation of aerosol mass

As discussed in section 4(b), clouds are effective at convective redistribution of aerosol to the mid- and upper troposphere. Since mid-tropospheric aerosol concentrations at CCN sizes are typically much lower than those at the surface, the question arises as to what role mid-tropospheric aerosols, which were previously activated and later detrained and re-entrained into the cloud, play in cloud development. This question also has a bearing on the potential role of mid-tropospheric transported aerosol layers on cloud evolution. To examine this further, we have performed a sensitivity test, ST3, in which the aerosol regeneration process is purposely switched off. Although this is a rather unrealistic scenario, because it effectively removes aerosol particles from the system, it does provide a useful upper bound on the importance of the role of regeneration
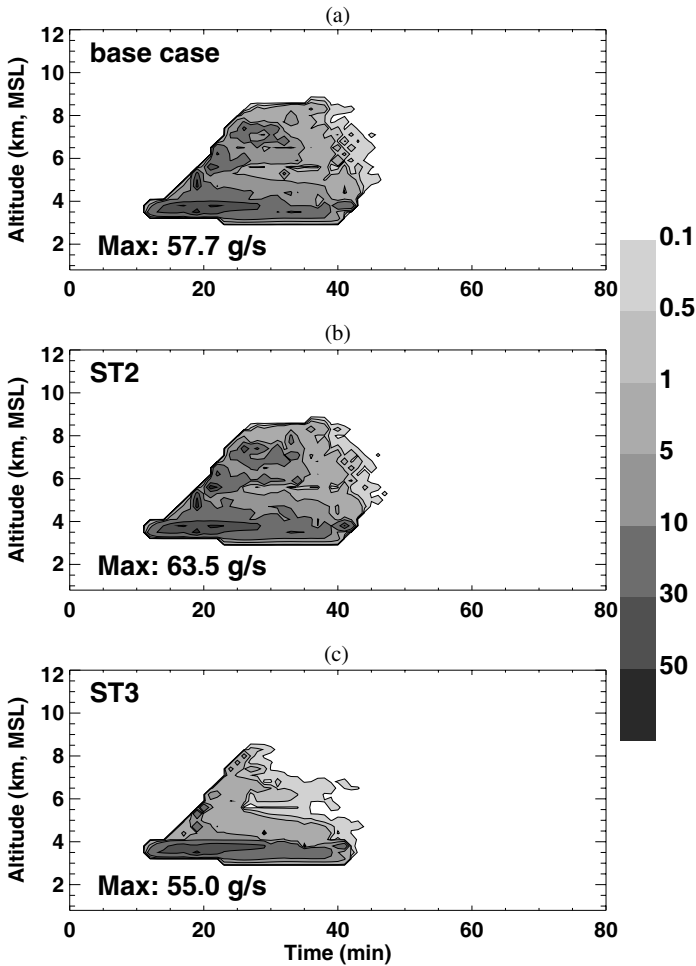
Figure 8.   Rates of change of integrated aerosol mass in hydrometeors through drop activation. The results are shown for (a) the base case, (b) the more polluted case (ST2), and (c) the case without aerosol regeneration (ST3).

and subsequent re-entrainment and activation of aerosol. Figure 8 shows the aerosol activation rate in this case as compared with the base case. It is clear that cloud processing (i.e. detrainment followed by entrainment) provides an increased concentration of CCN for in-cloud activation. The aerosol budget is given in Table 6. In the case where aerosol is allowed to be regenerated and re-entrained (the base case), 256 kg of aerosol acts as CCN and is nucleation scavenged, while switching off the regeneration/re-entrainment of processed aerosol (ST3) reduces this to 152 kg (note that in case ST3 the background aerosols are still entrained). Thus, 41% of the activated aerosol mass in the base case derives from re-entrained, processed aerosol. This sensitivity test shows that the additional activation in the base case arises from the re-entrainment of much higher aerosol masses, which can be attributed to production of aerosol at mid-cloud levels from hydrometeor evaporation. The small amount of ongoing activation above cloud base when regeneration is switched off (case ST3) is due to the higher supersaturation at mid-cloud levels (Fig. 5). The additional mass of aerosol that can be activated at the elevated supersaturations is evidently small compared with the additional mass that

is activated due to re-entrained processed aerosol. In any natural situation, the relative contribution of cloud processed aerosol will depend on the vertical profile of aerosol mass and number.

The concentration of additional CCN produced by re-entrainment of processed aerosol is in general dependent on the size distribution that is assumed for the evaporated aerosol (see section 2(e)). To test this, we have re-run the model assuming that the detrained aerosol is represented by a gamma function or a single size bin with the diameter equal to the volume-mean diameter of all the regenerated particles. The change in the CCN concentration, as derived from the maximum droplet concentration, is within $\pm 1\%$. This is likely because the regenerated aerosol mass typically resides at a size significantly larger than the minimum activated aerosol size. The lack of detail in the size distribution of regenerated particles that is inherent to Eulerian models appears not to be an important factor. We therefore believe that the change in CCN shown in Fig. 8 is a robust result.

(e)   Conceptual view of cloud processing of aerosol

Based on the above discussion we offer a conceptual view of the cloud processing of aerosols. Figure 9 shows schematically how the CCN budget is determined by the initial aerosol, vertical transport, the cloud-processed aerosol and the in-cloud oxidation of SO_2. Convection results in the vertical transport of aerosol-rich boundary-layer air into the cloud. Sub-cloud aerosol directly affects the number of activated cloud droplets at cloud base where supersaturation is high; at mid- and upper levels detrained, cloud-processed aerosol can be re-entrained into the cloud and contribute to further activation, although reduced in magnitude, particularly later on in the cloud development (Fig. 8). The extent of reactivation will depend on both the number and sizes of re-entrained aerosol as well as the supersaturation profile, which is dictated by dynamics. Contributions of sulphate chemistry to the aerosol embedded in the hydrometeors increases with increasing SO_2 and oxidant concentrations but has only a minor effect on cloud microphysics and precipitation formation. 'Internal' redistribution of aerosol through convective transport, collision–coalescence, regeneration, and re-entrainment are significantly more important than aerosol mass addition through aqueous chemistry.

(f)   Effect of processed aerosol on cloud microphysics

How do the cloud-processed aerosols influence the subsequent development of cloud properties and precipitation? Previous studies (e.g. Feingold *et al.* 1996; Wurzler *et al.* 2000; and Yin *et al.* 2002b) discussed the possible effects of cloud processing on subsequent cloud cycles. Feingold and Kreidenweis (2002) discussed effects on the primary cloud but for warm processes only. Here we examine the effects on the primary cloud for both warm and cold processes. Simulation ST3 has lower aerosol than the base case and offers an interesting comparison regarding the sensitivity of cloud evolution to aerosol loading. In the case of ST3, the changes to aerosol loading derive from neglect of the regeneration process that removes aerosol from the system and reduces re-entrainment at mid-levels. It is instructive to examine how the neglect of these processes influences the cloud evolution.

Figure 10 compares the concentrations of droplets, ice crystals and graupel production in case ST3 and the base case. It is clear that re-entrainment of cloud processed aerosol in the base case leads to more effective CCN which in turn leads to an increase in cloud droplet concentration from 897 to 930 cm^{-3}. On the other hand, the maximum production of ice particles in the base case, 1763 and 5.8 l^{-1} for ice crystal and graupel, respectively, is lower than in case ST3, 2430 and 9.9 l^{-1}, respectively.
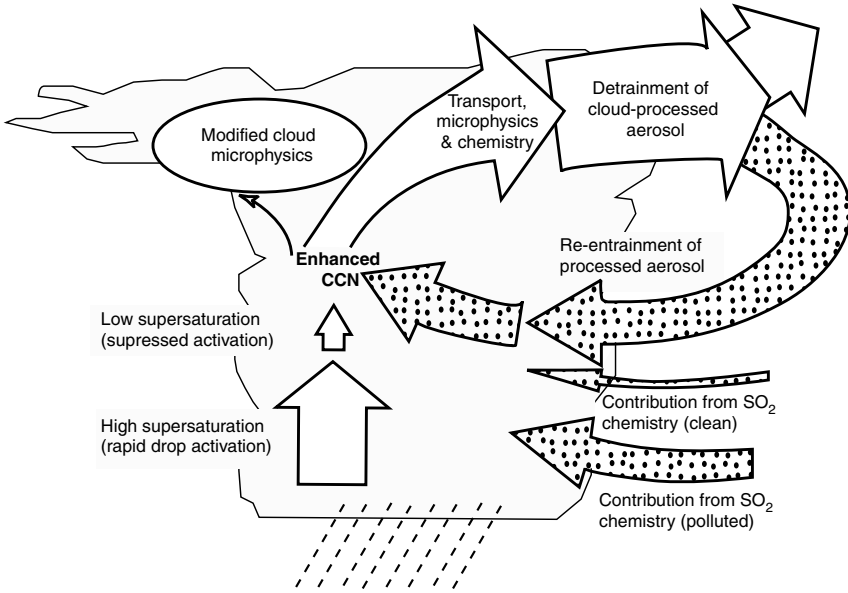
Figure 9.   Schematic of the processes described in this paper. Aerosol activated to cloud drops at cloud base is enhanced by re-entrained cloud-processed aerosol. The width of the arrows indicates the approximate budget of CCN-sized aerosol.
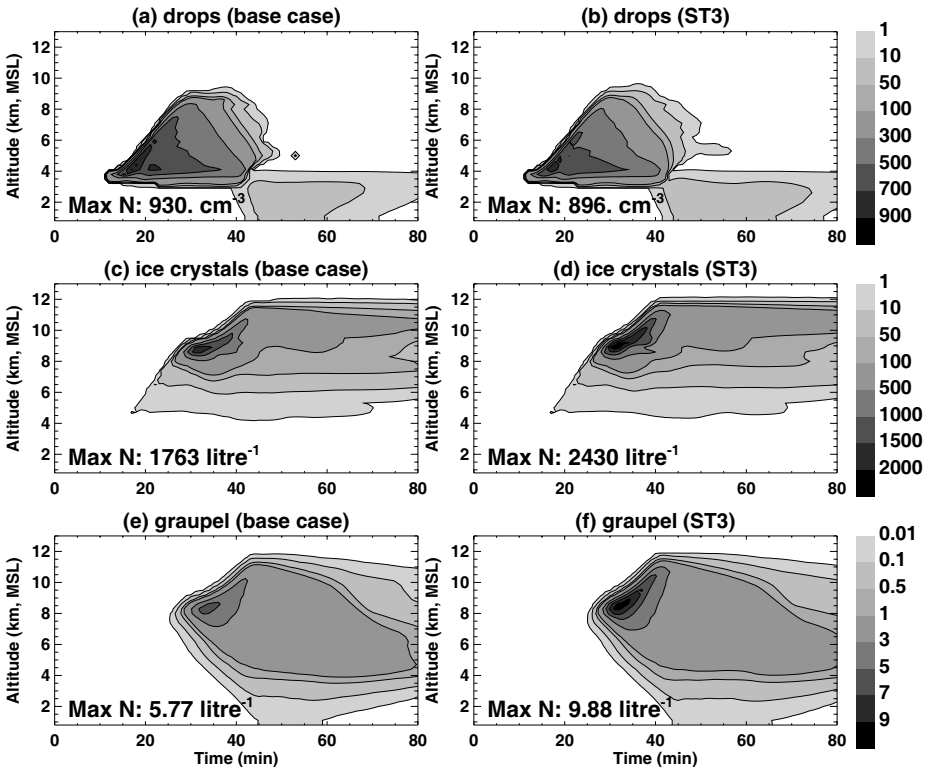
Figure 10.   Evolution of maximum concentrations of cloud droplets, ice crystals and graupel particles from the base case and case ST3 at different altitudes.

A detailed analysis of the microphysical processes in these two cases indicates that drop freezing and water-vapour deposition (or condensation freezing) are the dominant processes for ice production, while drop freezing as well as coagulation between drops and ice-phase particles are responsible for graupel production. Both these processes are more pronounced in case ST3 than in the base case. This can be explained by the fact that the higher population of cloud droplets in the base case leads to stronger competition for available water vapour during condensational growth, which could limit ice nucleation through deposition. On the other hand, the relatively fast growth of water droplets in case ST3 results in more efficient production of frozen drops (either ice crystals or graupel, depending on their size). The freezing process included in this model, is a parametrization based on the laboratory experiments of Bigg (1953), and predicts freezing rates that are strongly dependent on drop size (Pruppacher and Klett 1997). Changes in cloud microphysical processes by the cloud-processed aerosol particles, as discussed above, also affect precipitation. In the base case the integrated rain amount on the ground is 2.5×10^7 kg, which is 37% lower than that in case ST3 (3.9×10^7 kg). The microphysical responses of the simulated cloud to changes in droplet concentrations are generally consistent with those calculated in other model studies (Khain *et al.* 1999; Phillips *et al.* 2002) but much further work is needed to examine the sensitivity of ice microphysical response to the change in aerosol concentrations.

5. SUMMARY AND CONCLUSIONS

An axisymmetric dynamic cloud model with bin-resolved microphysics and chemistry has been developed and used to investigate the effects of mixed-phase convective clouds on scavenging, processing and vertical redistribution of atmospheric sulphate particles in the troposphere. In particular, we have examined the relative importance of nucleation scavenging, impaction scavenging, evaporation, and aqueous-phase chemistry for the aerosol budget in hydrometeors. We have also examined the feedback of the cloud-processed aerosols on development of cloud microphysical properties and precipitation in a moderately deep convective cloud that occurred on 19 July 1981 near Miles City, Montana, during the Cooperative Convective Precipitation Experiments. This is the first time that a dynamical mixed-phase cloud model with bin-resolved microphysics and chemistry has been used to simulate a real case. A comparison between the model cloud and available observations demonstrates that the model reproduces reasonably well the macro- and micro-structure of the observed cloud. As in earlier studies, we find that nucleation scavenging (drop activation) dominates the in-cloud scavenging processes, while impaction scavenging plays a minor role inside clouds and only becomes important below cloud base. Aqueous production of sulphate accounts for a relatively small amount of in-cloud sulphate (<17% for the cases simulated here). Twin simulations with and without aqueous chemistry show that this process does not affect the evolution of the cloud or its propensity to precipitate.

Our simulations show that re-entrained, processed aerosol may add significantly to the CCN budget in the middle and upper region of convective clouds. The precise CCN budget will depend on the sizes of aerosols detrained, the extent to which the detrained air is re-entrained during cloud development, and the dynamically produced supersaturation. As shown here, the re-entrained processed CCN may modify the cloud microphysical evolution quite significantly by delaying drop freezing and/or limiting ice-crystal growth. The result of neglecting the re-entrainment of processed CCN is a significant increase in precipitation (37% for the case simulated here). The demonstrated potential for mid-level aerosol activation suggests that the occurrence of

mid-tropospheric aerosol layers that have been advected by long-range transport could strongly affect cloud evolution. The effects on the cloud could be even more complicated if these particles are effective ice nuclei (e.g. Sassen *et al.* 2003). Most convective cloud models do not treat aerosol with much detail and most do not carry soluble material as a prognostic variable. Our simulations show that these are likely to be important quantities in any simulation of cloud evolution.

It should be borne in mind that the treatment of regenerated aerosol in this work has it limitations, as described in section 2(e). Nevertheless, our results do not show sensitivity to the assumed size distribution of regenerated particles around the (resolved) mean size. Regarding regeneration of aerosol following evaporation of ice crystals, our results are only weakly sensitive to the assumed number of regenerated particles over the range 1–10 cm^{-3} because the concentration of ice particles is two to three orders of magnitude smaller than that of the ambient aerosol. We are therefore confident that the results presented here are not compromised by the treatment of regeneration. To explicitly track the individual aerosol particles is impractical in such a mixed-phase cloud due to the nonlinear interactions among various cloud particles.

It is well known that convective clouds have a significant effect on the tropospheric aerosol budget through the process of precipitation scavenging. This work also elucidates the details of how convective clouds transport aerosols from the boundary layer up to the mid-/upper troposphere. As shown in Fig. 6, tropospheric aerosol mass and number concentrations at 11 km are increased by factors of about 2–3 relative to background values and aerosol surface area is increased by a similar amount, although the fractional changes at any one location will depend on the local vertical profile of aerosol. This vertical redistribution may have an important impact on aerosol direct and indirect effects by scattering solar radiation and supplying nuclei for ice clouds. Increased aerosol surface area may enhance surface reactions on particles. Furthermore, convective transport also facilitates horizontal transportation by the high ambient winds characteristic of the mid-/upper troposphere. Further aspects of this problem will be addressed in forthcoming studies.

REFERENCES

Alheit, R. R., Flossmann, A. I. and Pruppacher, H. R. 1990 A theoretical study of the wet removal of atmospheric pollutants, IV: The uptake and redistribution of aerosol particles through nucleation and impaction scavenging by growing cloud drops and ice particles. *J. Atmos. Sci.*, **47,** 870–887

Beard, K. V. and Grover, S. N. 1974 Grover, numerical collision efficiencies for small raindrops colliding with micro size particles. *J. Atmos. Sci.*, **31,** 543–550

Bigg, E. K. 1953 The formation of atmospheric ice crystals by the freezing of droplets. *Q. J. R. Meteorol. Soc.*, **79,** 510–519

Bower, K. N. and Choularton, T. W.   1993   Cloud processing of the cloud condensation nucleus spectrum and its climatological consequences. *Q. J. R. Meteorol. Soc.*, **119,** 655–679

Bower, K. N., Choularton, T. W., Gallagher, M. W., Colvile, R. N., Wells, M., Beswick, K. M., Wiedensohler, A., Hansson, H.-C., Svenningsson, B., Swietlicki, E., Wendisch, M., Berner, A., Kruisz, C., Laj, P., Facchini, M. C., Fuzzi, S., Bizjak, M., Dollard, G., Jones, B., Acker, K., Wieprecht, W., Preiss, M., Sutton, M. A., Hargreaves, K. J., Storeton-West, R. L., Cape, J. N. and Arends, B. G.   1997   Observations and modeling of the processing of aerosol by a hill cap cloud. *Atmos. Environ.*, **31,** 2527–2543

Choularton, T. W., Bower, K. N., Beswick, K. M., Parkin, M. and Kaye, A.   1998   A study of the effects of cloud processing of aerosol on the microphysics of cloud. *Q. J. R. Meteorol. Soc.*, **124,** 1377–1389

Dickerson, R. R., Huffman, G. J., Luke, W. T., Nunnermacker, L. J., Pickering, K. E., Leslie, A. C. D., Lindsey, C. G., Slinn, W. G. N., Kelly, T. J., Daum, P. H., Delany, A. C., Greenberg, J. P., Zimmerman, P. R., Boatman, J. F., Ray, J. D. and Stedman, D. H.   1987   Thunderstorms: An important mechanism in the transport of air pollutants. *Science*, **235,** 460–465

Dye, J. E., Jones, J. J., Winn, W. P., Cerni, T. A., Gardiner, B., Lamb, D., Pitter, R. L., Hallet, J. and Saunders, C. P. R.   1986   Early electrification and precipitation development in a small, isolated Montana cumulonimbus. *J. Geophys. Res.*, **91,** 1231–1247

Feingold, G. and Kreidenweis, S. M.   2002   Cloud processing of aerosol as modeled by a large eddy simulation with coupled microphysics and aqueous chemistry. *J. Geophys. Res.*, **107**(D23)**,** 4687, doi: 10.1029/2002JD002054

Feingold, G., Tzivion, S. and Levin, Z.   1988   The evolution of raindrop spectra. Part I: Stochastic collection and breakup. *J. Atmos. Sci.*, **45,** 3387–3399

Feingold, G., Kreidenweis, S. M., Stevens, B. and Cotton, W. R.   1996   Numerical simulation of stratocumulus processing of cloud condensation nuclei through collision-coalescence. *J. Geophys. Res.*, **101,** 21391–21402

Flossmann, A. I. and Pruppacher, H. R.   1988   A theoretical study of the wet removal of atmospheric pollutants. Part III: The uptake, redistribution, and deposition of $(NH_4)_2SO_4$ particles by a convective cloud using a two-dimensional cloud dynamic model. *J. Atmos. Sci.*, **45,** 1857–1871

Flossmann, A. I., Hall, W. D. and Pruppacher, H. R.   1985   A theoretical study of the wet removal of atmospheric pollutants. Part I: The redistribution of aerosol particles captured through nucleation and impaction scavenging by growing cloud drops. *J. Atmos. Sci.*, **42,** 582–606

Georgii, H. W. and Meixner, F. X.   1980   Measurement of the tropospheric and stratospheric SO_2 distribution. *J. Geophys. Res.*, **85,** 7433–7438

Hatzianastassiou, N., Wobrock, W. and Flossmann, A. I.   1998   The effect of cloud-processing of aerosol particles on clouds and radiation. *Tellus*, **50B,** 478–490

Hegg, D. A. and Hobbs, P. V.   1982   Measurement of the sulphate production in natural clouds. *Atmos. Environ.*, **16,** 2663–2668

Hegg, D. A., Hobbs, P. V. and Radke, L. F.   1984   Measurements of the scavenging of sulphate and nitrate in clouds. *Atmos. Environ.*, **18,** 1939–1946

Helsdon, J. H. and Farley, R. D.	1987	A numerical modeling study of a Montana thunderstorm: 1. Model results versus observations involving nonelectrical aspects. *J. Geophys. Res.*, **92**, 5645–5659
Hobbs, P. V., Bowdle, D. A. and Radke, L. F.	1985	Particles in the lower troposphere over the high plains of the United States. Part I: Size distributions, elemental composition and morphologies. *J. Clim. Appl. Meteorol.*, **24**, 1344–1356
Hoffmann, M. R. and Calvert, J. G.	1985	*Chemical transformation modules for Eulerian acid deposition models*, Volume 2. *The aqueous-phase chemistry.* EPA/600/3-85/017. US Environment Protection Agency, Research Triangle Park, NC, USA
Hudson, J. G.	1993	Cloud condensation nuclei near marine cumulus, *J. Geophys. Res.*, **98**, 2693–2702
Iribarne, J. V., Pyshnov, T. and Naik, B.	1990	The effect of freezing on the composition of supercooled droplets, II. Retention of SO_2. *J. Atmos. Environ.*, **24A,** 389–395
Jacob, D. J.	1986	Chemistry of OH in remote clouds and its role in the production of formic acid and peroxymonosulphate. *J. Geophys. Res.*, **91**, 9807–9826
Jensen, J. B. and Charlson, R. J.	1984	On the efficiency of nucleation scavenging. *Tellus*, **36B**, 367–375
Junge, C. E.	1963	*Air chemistry and radioactivity*, Academic Press, New York
Khain, A., Pokrovsky, A. and Sednev, I.	1999	Some effects of cloud-aerosol interaction on cloud microphysics structure and precipitation formation: Numerical experiments with a spectral microphysics cloud ensemble model. *Atmos. Res.*, **52,** 195–220
Kleinman, L. I. and Daum, P. H.	1991	Vertical distribution of aerosol particles, water vapor, and insoluble trace gases in convectively mixed air. *J. Geophys. Res.*, **96**, 991–1005
Kogan, Y. L.	1991	The simulation of a convective cloud in a 3-D model with explicit microphysics. Part I: Model description and sensitivity experiments. *J. Atmos. Sci.*, **48**, 1160–1189
Kreidenweis, S. M., Zhang, Y. and Taylor, G. R.	1997	The effects of clouds on aerosol and chemical species and production and distribution. 2: Chemistry model description and sensitivity analysis. *J. Geophys. Res.*, **102**, 23867–23882
Lide, D. R. and Frederikse, H. P. R.	1995	*CRC handbook of chemistry and Physics,* 76th edition. CRC Press, Inc., Boca Raton, FL, USA
Luke, W. T., Dickerson, R. R., Ryan, W. F., Pickering, K. E. and Nunnermacker, L. J.	1992	Nunnermacker, tropospheric chemistry over the lower great plains of the United States, 2: Trace gas profiles and distributions. *J. Geophys. Res.*, **97**, 20647–20670
McArdle, J. V. and Hoffmann, M. R.	1983	Kinetics and mechanism of the oxidation of aquated sulfur dioxide by hydrogen peroxide at low pH. *J. Phys. Chem.*, **87,** 5425–5429
Martin, J. J., Wang, P. K. and Pruppacher, H. R.	1980	A theoretical determination of the efficiency with which aerosol particles are collected by simple ice crystal plates. *J. Atmos. Sci.*, **37**, 1628–1638
Mitra, S. K., Pruppacher, H. R. and Brinkmann, J.	1992	A wind tunnel study on the drop-to-particle conversion. *J. Aerosol Sci.*, **23**, 245–256
Mordy, W.	1959	Computation of the growth by condensation of a population of cloud droplets. *Tellus*, **11**, 16–44
Murakami, M.	1990	Numerical modeling of dynamical and microphysical evolution of an isolated convective cloud. The 19 July 1981 CCOPE cloud. *J. Meteorol. Soc. Jpn.*, **68**, 107–128
Murakami, M., Kikuchi, K. and Magono, C.	1985	Experiments on aerosol scavenging by natural snow crystals. Part I: Collection efficiency of uncharged snow crystals by submicron particles. *J. Meteorol. Soc. Jpn.*, **63**, 119–129
O'Sullivan, D. W., Lee, M., Noone, B. C. and Heikes, B. G.	1996	Henry's law constant determinations for hydrogen peroxide, methyl hydroperoxide, hydroxymethyl hydroperoxide, ethyl hydroperoxide, and peroxyacetic acid. *J. Phys. Chem.*, **100**, 3241–3247
Perrin, D. D.	1982	*Ionization constants of inorganic acids and bases in aqueous solution*, 2nd edition. Pergamon, New York
Phillips, V. T. J., Choularton, T. W., Blyth, A. M. and Latham, J.	2002	The influence of aerosol concentrations on the glaciation and precipitation of a cumulus cloud. *Q. J. R. Meteorol. Soc.*, **128,** 951–971
Pinsky, M. B. and Khain, A. P.	2002	Effects of in-cloud nucleation and turbulence on droplet spectrum formation in cumulus clouds. *Q. J. R. Meteorol. Soc.*, **128,** 501–533

Prather, M. J. and Jacob, D. J.	1997	A persistent imbalance in HO_x and NO_x photochemistry of the upper troposphere driven by deep tropical convection. *Geophys. Res. Lett.*, **24,** 3189–3192
Pruppacher, H. R. and Klett, J. D.	1997	*Microphysics of clouds and precipitation.* D. Reidel, Amsterdam
Reisin, T., Levin, Z. and Tzivion, S.	1996	Rain production in convective clouds as simulated in an axisymmetric model with detailed microphysics. Part I: Description of the model. *J. Atmos. Sci.*, **53,** 497–519
Respondek, P. S., Flossmann, A. I., Alheit, R. R. and Pruppacher H. R.	1995	A theoretical study of the wet removal of atmospheric pollutants. Part V: The uptake, redistribution, and deposition of $(NH_4)_2SO_4$ by a convective cloud containing ice. *J. Atmos. Sci.*, **52,** 2121–2132
Rodhe, H.	1983	'Precipitation scavenging and tropospheric mixing'. Pp. 719–730 in *Precipitation scavenging, dry deposition and resuspension.* Eds. H. R. Pruppacher, R. G. Semonin and W. G. N. Slinn. Elsevier, New York
Sassen, K., DeMott, P. J., Prospero, J. M. and Poellot, M. R.	2003	Saharan dust storms and indirect aerosol effects on clouds: CRYSTAL-FACE results. *Geophys. Res. Lett.*, **30,** 1633–1636
Schumann, T., Zinder, B. and Waldvogel, A.	1988	Aerosol and hydrometeor concentrations and their chemical composition during winter precipitation above a mountain slope. *Atmos. Environ.*, **22,** 1443–1459
Seinfeld, J. H. and Pandis, S. N.	1998	*Atmospheric chemistry and physics: From air pollution to climate change.* John Wiley & Sons, Inc., New York
Smith, R. M. and Martell, A. E.	1976	*Critical stability constants.* Vol. 4: *Inorganic complexes.* Plenum Press, New York
Snider, J. R., Montague, D. C. and Vali, G.	1992	Hydrogen peroxide retention in rime ice. *J. Geophys. Res.*, **97,** 7569–7578
Taylor, G. R., Kreidenweis, S. M. and Zhang, Y.	1997	The effects of clouds on aerosol and chemical species and production and distribution. 1: Cloud model formation, mixing, and detrainment. *J. Geophys. Res.*, **102,** 23851–23865
Tzivion, S., Feingold, G. and Levin, Z.	1987	An efficient numerical solution to the stochastic collection equation. *J. Atmos. Sci.*, **44,** 3139–3149
	1989	The evolution of raindrop spectra. Part II: Collisional collection/breakup and evaporation in a rainshaft. *J. Atmos. Sci.*, **46,** 3312–3327
Tzivion, S., Reisin, T. and Levin, Z.	1994	Numerical simulation of hygroscopic seeding in a convective cloud. *J. Appl. Meteorol.*, **33,** 252–267
Wang, P. K. and Pruppacher, H. R.	1977	An experimental determination of the efficiency with which aerosol particles are collected by water drops in subsaturated air. *J. Atmos. Sci.*, **34,** 1664–1669
Wang, P. K., Grover, S. N. and Pruppacher, H. R.	1978	On the effect of electric charges on the scavenging of aerosol particles by cloud and small rain drops. *Atmos. Res.*, **35,** 1735–1743
Wurzler, S., Reisin, T. G. and Levin, Z.	2000	Modification of mineral dust particles by cloud processing and subsequent effects on drop size distributions. *J. Geophys. Res.*, **105,** 4501–4512
Yin, Y., Parker, D. J. and Carslaw, K. S.	2001	Simulation of trace gas redistribution by convective clouds—Liquid phase processes. *Atmos. Chem. Phys.*, **1,** 19–36
Yin, Y., Carslaw, K. S. and Parker, D. J.	2002a	Redistribution of trace gases by convective clouds—Mixed-phase processes. *Atmos. Chem. Phys.*, **2,** 293–306
Yin, Y., Wurzler, S., Levin, Z. and Reisin, T. G.	2002b	Interactions of mineral dust particles and clouds: Effects on precipitation and cloud optical properties. *J. Geophys. Res.*, **107**(D23)**,** 4724, doi: 10.1029/2001JD001544
Yuen, P.-F., Hegg, D. A. and Larson, T. V.	1994	The effects of in-cloud sulphate production on light-scattering properties of continental aerosol. *J. Appl. Meteorol.*, **33,** 848–854